

Structural behavior of sandwich composite wall with truss connectors under compression

Ying Qin^{*1,2}, Xin Chen², Xingyu Zhu², Wang Xi² and Yuanze Chen²

¹Key Laboratory of Concrete and Prestressed Concrete Structures of Ministry of Education, Southeast University, Nanjing, China

²School of Civil Engineering, Southeast University, Nanjing, China

(Received November 23, 2019, Revised February 4, 2020, Accepted March 4, 2020)

Abstract. Sandwich composite wall consists of concrete core attached by two external steel faceplates. It combines the advantage of steel and concrete. The appropriate composite action between steel faceplate and concrete core is achieved by using adequate mechanical connectors. This research studied the compressive behavior of the sandwich composite walls using steel trusses to bond the steel faceplates to concrete infill. Four short specimens with different wall width and thickness of steel faceplate were designed and tested under axial compression. The test results were comprehensively evaluated in terms of failure modes, load versus axial and lateral deformation responses, resistance, stiffness, ductility, strength index, and strain distribution. The test results showed that all specimens exhibited high resistance and good ductility. Truss connectors offer better restraint to walls with thinner faceplates and smaller wall width. In addition, increasing faceplate thickness is more effective in improving the ultimate resistance and axial stiffness of the wall.

Keywords: sandwich composite; truss connector; compression; structural behavior

1. Introduction

Sandwich composite wall is a novel form of wall system which consists of two external steel faceplates and plain concrete infill. It has been researched for application in building structures (Curkovic *et al.* 2019), blast-resistant system (Bruhl and Varma 2018), and offshore protective platforms (Wei *et al.* 2019). Similar to conventional reinforced concrete walls (Bafti *et al.* 2019, Beiraghi 2019), composite beams (Yang *et al.* 2018, Varshney *et al.* 2019, Song *et al.* 2019), and concrete filled tubular columns (Deifalla *et al.* 2019, Zhou *et al.* 2019), sandwich composite walls combine the advantage of the ductility of steel (Liu *et al.* 2018) with the compressive strength of concrete. The steel faceplates serve as the primary reinforcement for concrete. However, sandwich composite walls exhibit better capacity and ductility characteristics.

During the construction stage, steel faceplates will function to stabilize the structural frame once they are erected on site. They also act as permanent formwork for casting the infill concrete. During the service stage, the axial and lateral loads will be carried by both steel faceplates and concrete core. Composite action between the steel faceplates and infill concrete is achieved by embossments or various forms of connectors such as shear studs (Hu *et al.* 2014) and tie bars (Ayazi and Shafaei 2019).

Previous research on sandwich composite walls subjected to axial compression and in-plane shear force showed that adequate mechanical interlock at the steel-

concrete interface is essential to ensure the composite action and achieve good structural behavior (Hossain and Wright 2004, Rafiei *et al.* 2017). Such research also confirmed that sandwich composite wall can be potentially used as the suitable alternative to reinforced concrete wall (Mydin and Wang 2011, Prabha *et al.* 2013, Huang and Liew 2016).

In this research, a novel type of sandwich composite wall system proposed by Qin *et al.* (2019a) was studied. Steel trusses were attached to the interior surface of steel faceplates to serve as the mechanical connectors, as shown in Fig. 1. Truss connectors can not only provide strong restraint to steel plates but also ensure the ductile mode of failure of such composite wall. It should be noted that the steel trusses are welded to the steel faceplates by automatic machines with foldable arms in the factory, which saves labor and time. The two external steel faceplates, which are connected by truss connectors, are then delivered to the site as a unite.

Extensive work has been conducted on sandwich composite walls to study their in-plane shear behavior (Nie *et al.* 2014, Seo *et al.* 2016, Yan *et al.* 2018), seismic behavior (Eom *et al.* 2009, Chen *et al.* 2015, Zhao *et al.* 2016, Ji *et al.* 2017, Nguyen and Whittaker 2017, Guo *et al.* 2018, Huang *et al.* 2018, Chen *et al.* 2019), impact resistance (Bruhl and Varma 2018, Guo and Zhao 2019) and fire resistance (Rafiei *et al.* 2017, Wei *et al.* 2019). Some studies have been performed on the compressive performance of such walls with shear studs (Mydin and Wang 2011, Prabha *et al.* 2013, Choi *et al.* 2014, Yan *et al.* 2019). The structural behavior of truss connectors is believed to be different from shear studs. The shear studs can offer point restraints to the external faceplates, while the steel trusses provide line restraints along the length of trusses.

*Corresponding author, Associate Professor
E-mail: qinying@seu.edu.cn

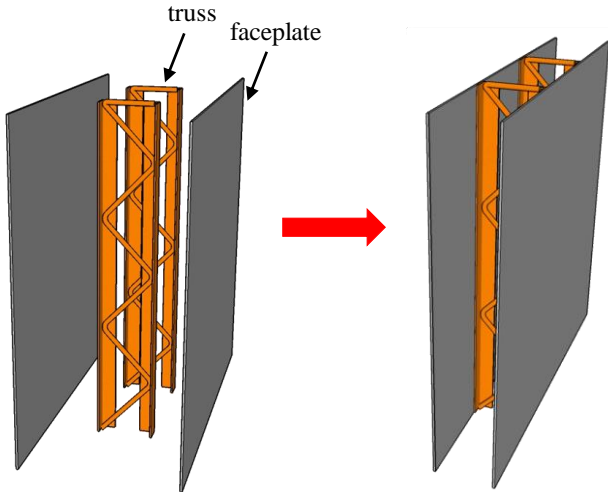


Fig. 1 Sandwich composite wall with truss connectors

Therefore, the truss connector is expected to offer better confinement to steel faceplates along the longitudinal direction and exhibit better performance. Until to data very limited research has been done on the sandwich composite wall with truss connectors. Most of the studies are focusing on high walls (Qin *et al.* 2019a, b), while some study is associated with short walls (Qin *et al.* 2020). It can be expected that the behavior of short walls would be different from high walls due to the lack of overall buckling.

This paper describes the axial loading behavior of sandwich composite short walls with truss connectors, based on comprehensively experimental investigation. The width of wall and the thickness of steel faceplate are the concern of current study. The influences of these parameters on resistance, failure modes, stiffness, ductility, and strain distribution are evaluated. The compressive resistances of the tested walls are compared with those obtained from modern codes. This research will contribute to better understanding of the potentials of the proposed composite wall system.

2. Experimental program

2.1 Specimen details

The test consists of four sandwich composite walls with truss connectors, i.e., CWT4W900, CWT4W1200, CWT4W600, and CWT8W900. Fig. 2 and Table 1 show the details of the tested specimens. Specimen CWT4W900 is the control specimen and has the height of 500 mm, width of 900 mm, and thickness of 150 mm. The height-to-thickness ratio is 3.33 and the wall is classified into short wall category, which means the failure of the wall is expected to be governed by cross-sectional capacity rather than global buckling. The thickness of steel faceplates is 4 mm. The steel trusses are composed of two angles with the size of L40×40×4 mm and curl bar with the diameter of 8 mm. The truss spacing is 200 mm, and the resulted ratio between the truss

spacing and steel faceplate thickness is $50\sqrt{235/f_y}$.

In order to study the influence of key parameters on compressive behaviour of sandwich composite walls with truss connectors, Specimens CWT4W1200 and CWT4W600 are designed with different width of 1200 mm and 600 mm, respectively. In addition, Specimen CWT8W900 is designed with different steel faceplate thickness of 8 mm compared with Specimen CWT4W900.

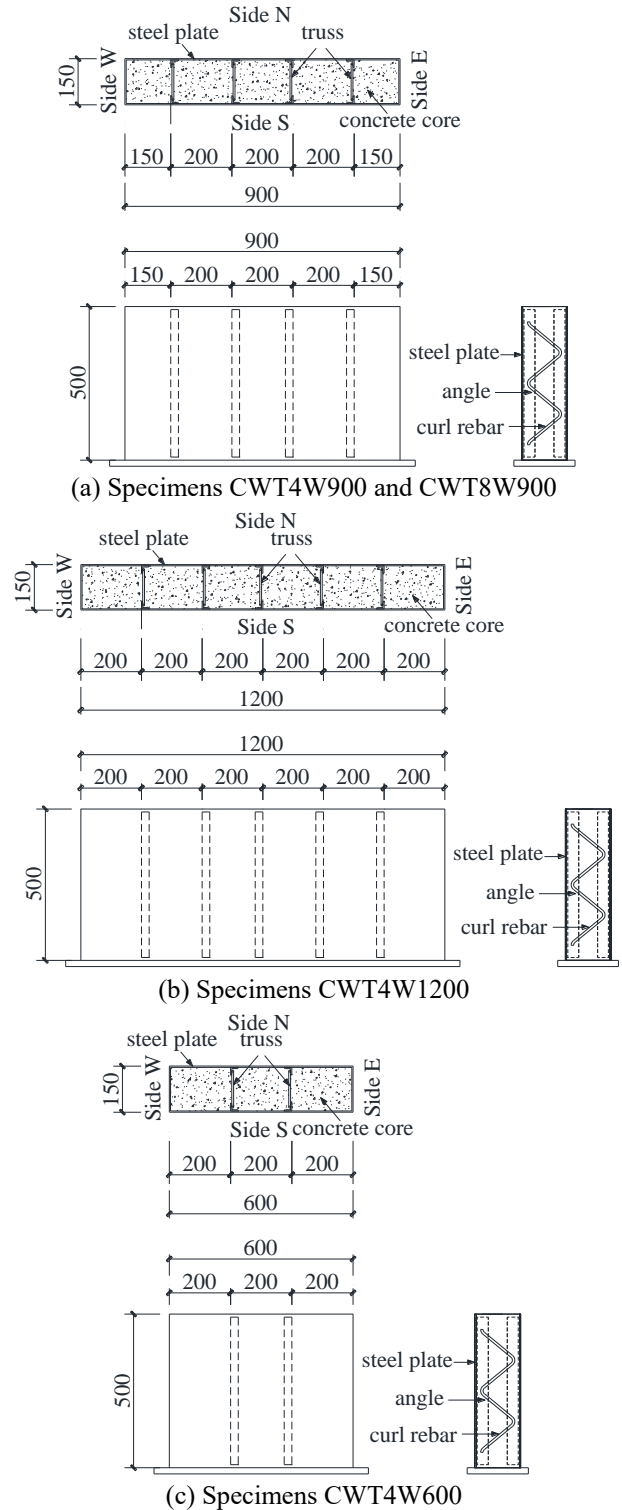


Fig. 2 Tested sandwich composite walls

Table 1 Specimen details

Specimen No.	h_w	L_w	b_w	t_s	d_s
	mm	mm	mm	mm	mm
CWT4W900	500	900	150	4	200
CWT4W1200	500	1200	150	4	200
CWT4W600	500	600	150	4	200
CWT8W900	500	900	150	8	200

Note: h_w , L_w and b_w are the height, length and width of sandwich composite wall; t_s is the thickness of steel plate; and d_s is the truss spacing

2.2 Material properties

In order to determine the material properties of steel faceplates, three tension coupon specimens per thickness are made from the same batch of steel faceplates used for the test specimens. For 4 mm thick steel faceplate, the average yield and ultimate strength of the steel faceplate are 346.0 MPa and 364.8 MPa, respectively. The average elastic modulus is 1.99×10^5 MPa. For 8 mm thick steel faceplate, the elastic modulus, yield strength, and ultimate strength were 2.12×10^5 MPa, 286.0 MPa, and 434.6 MPa, respectively.

Three cubes with the dimension of $150 \times 150 \times 150$ mm are cast and tested. The average cubic compressive strength is 23.9 MPa. The resulted cylinder compressive strength is 16.0 MPa, which is calculated by Eq. (1) based on GB 50010–2010 (2015) Code for design of concrete structures. It should be noted that concrete strength is relatively low in this research due to the limitation of loading capacity of testing machine. However, the concrete strength has more influence on the cross sectional capacity than on the composite action. The advantage of using this new composite wall for high strength concrete can be explored by more tests or finite element simulations.

$$f_c = 0.88\alpha_1\alpha_2f_{cu} \quad (1)$$

where f_c is the cylinder compressive strength of concrete, f_{cu} is the cubic compressive strength of concrete, α_1 is the ratio between the cylinder compressive strength and the cubic compressive strength and can be taken as 0.76 for concrete under C50, and α_2 is the reduction factor considering brittle behavior of concrete and can be taken as 1.0 for concrete under C40.

2.3 Test setup

Fig. 3 shows the test setup for the compressive tests on sandwich composite walls with truss connectors. All the specimens are placed directly to the rigid support of a 10000 kN loading machine. The positions of the specimens are carefully adjusted to ensure uniform axial compression without eccentricity. The specimens were loaded at the load interval of 250 kN for Specimen CWT4W600 and 500 kN for the other three specimens, and each load interval was maintained for 5 min. The loading intervals were selected based on three principles. Firstly, a minimum of seven loading steps should be applied until the tested wall reaches

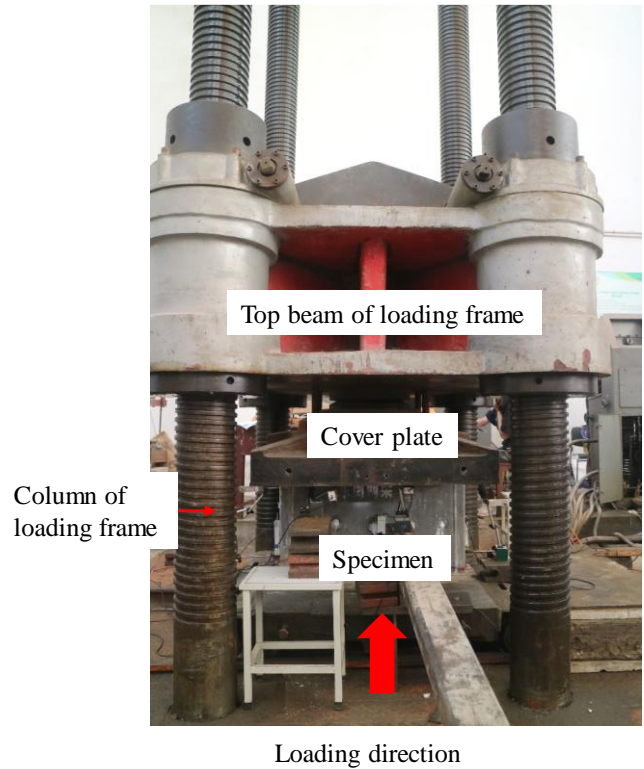


Fig. 3 Test setup

the ultimate compressive strength. Secondly, as many as specimens could share the same loading intervals. Thirdly, the applied loading is the multiples of fifty for convenience. Due to the monotonic loading characteristics in this test, the smaller loading intervals for Specimen CWT4W600 is expected to have small influence on test results as long as sufficient loading steps have been applied.

2.4 Instrumentations

Four displacement transducers (DTs) D1~D4 were vertically installed to obtain the axial displacement during the test. Six more DTs (D5~D10) were horizontally placed to measure the out-of-plane deflection. The installation of DTs for all specimens are shown in Fig. 4. Several strain gauges were arranged for each specimen to record the strains of the steel faceplates at different locations, as shown in Fig. 5.

3. Test results

3.1 Failure modes

Fig. 6 shows the failure modes for each tested specimen. Due to the small value of height-to-thickness ratio, global buckling was not observed in the test. All specimens reached their cross-sectional resistance. The steel faceplates experienced local buckling between the adjacent truss connectors before the failure. It can also be noticed that slight differences exist in the locations for the local buckling of the two side steel faceplates in most of the specimens.

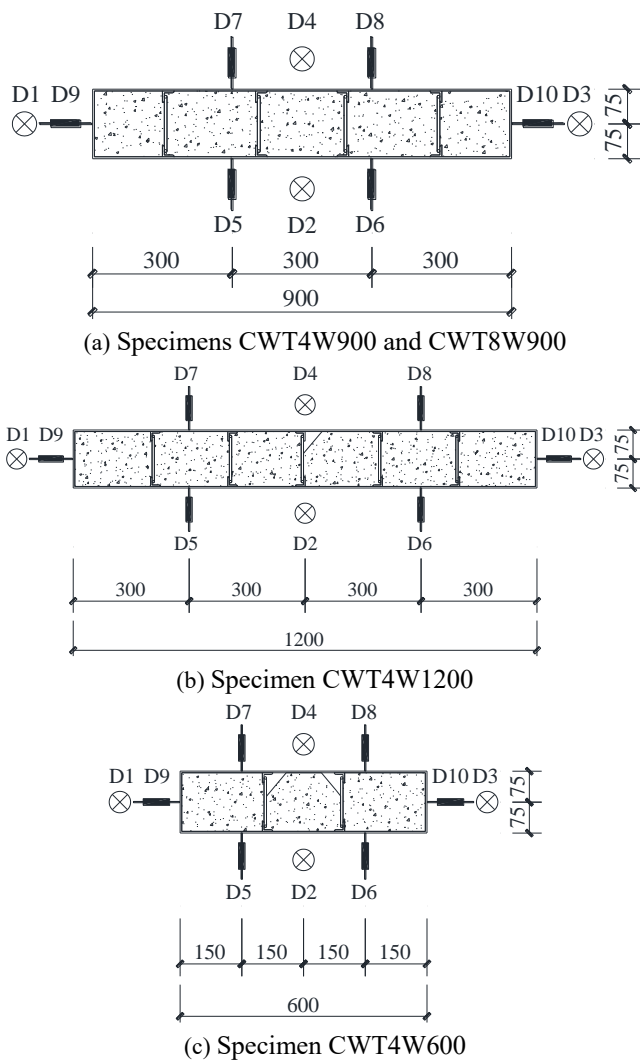


Fig. 4 Installation of DTs

This may be caused by slight load eccentricity and differences in initial imperfections on two sides. However, the buckling shapes of all specimens were quite similar. The specimens were finally failed and lost its capacity to resist axial load due to the combined buckling of steel faceplates and crushing of concrete core.

For Specimen CWT4W900, the steel faceplates started to buckle on side N as the specimen reached its 83% ultimate resistance (3000 kN). As the specimen reached its 97% ultimate resistance (3500 kN), steel plates on side W bulged out. Local buckling continued occurring to the steel faceplate on side S as the specimen arrived at its ultimate resistance.

For Specimen CWT4W1200, as the reaction force of the specimen equals to 73% its ultimate resistance (4500 kN), local buckling was found on side S. Continuous sound was emitted from the specimen, which was believed to be caused by the deforming of steel faceplates. The buckling gradually progressed to side N before the failure. The two short sides (sides W and E) were also bulged out when the specimen reached the ultimate resistance.

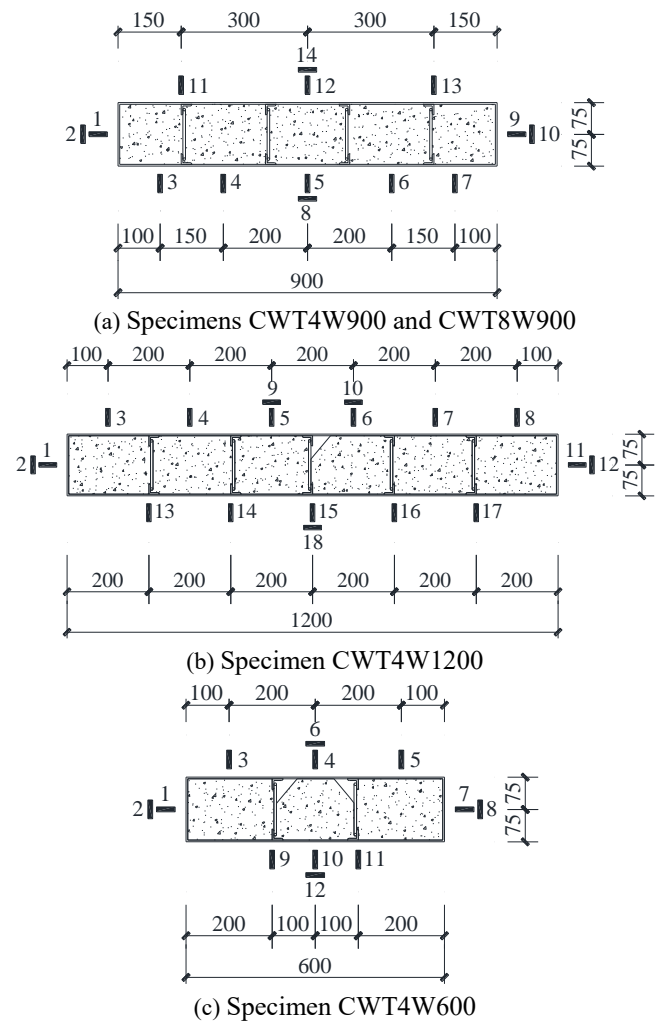
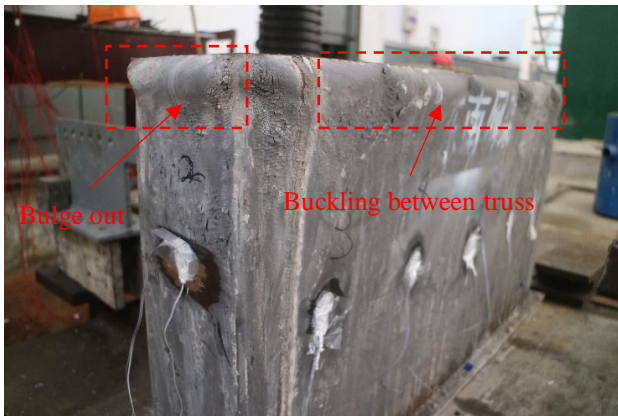


Fig. 5 Installation of strain gauges

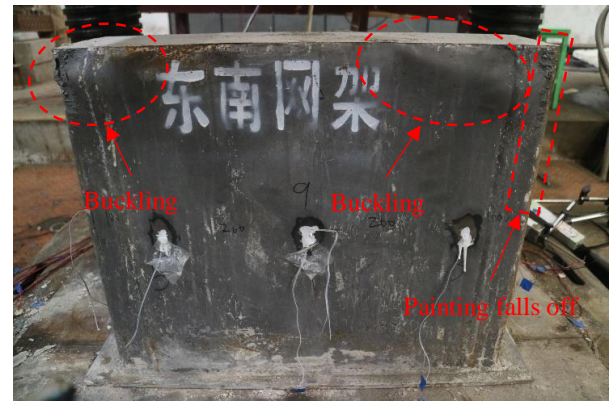
For Specimen CWT4W600, the steel faceplates near the top on side N exhibited slight local buckling at the 91% ultimate resistance (2500 kN). The buckling became severe and developed to the other three sides when reaching the ultimate resistance.

For Specimen CWT8W900, local buckling started to develop on side S as the specimen arrived at 75% its ultimate resistance (4500 kN). Gradually, steel faceplates on side W and E started to buckle. During the recession stage, the buckling on side N was observed as the load decreased to 90% its ultimate resistance (5400 kN).

The test observation shows that local buckling occurs earlier in Specimens CWT8W900 and CWT4W1200 than in the other two specimens. This indicates that the support of truss connectors to steel faceplates in the former two specimens is weaker. It can also be observed in Figs. 6(g) and (h) that the external steel faceplates of Specimen CWT8W900 buckled outwards as a whole, the locations where steel trusses were placed cannot be easily identified. This further demonstrates the poor restraint by the trusses.



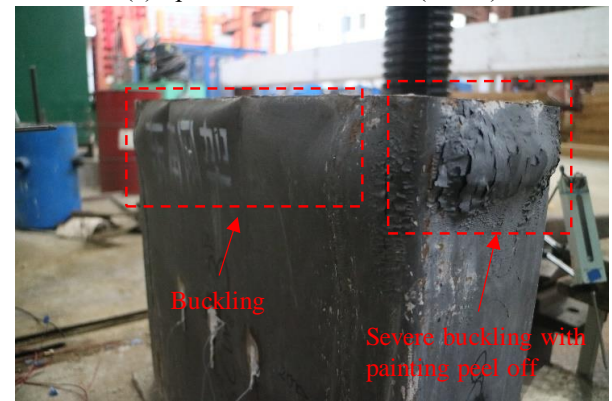
(a) Specimen CWT4W900 (Side S)



(e) Specimen CWT4W600 (side S)



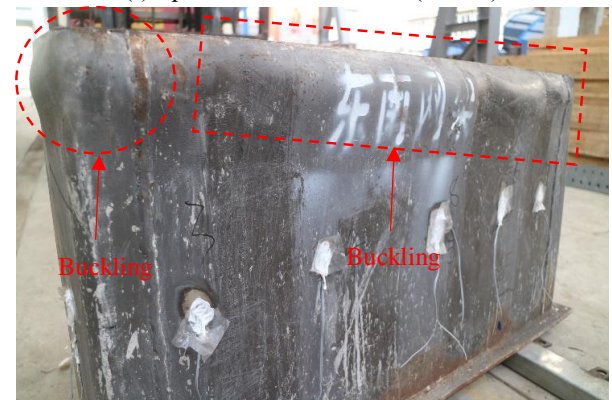
(b) Specimen CWT4W900 (side N)



(f) Specimen CWT4W600 (side N)



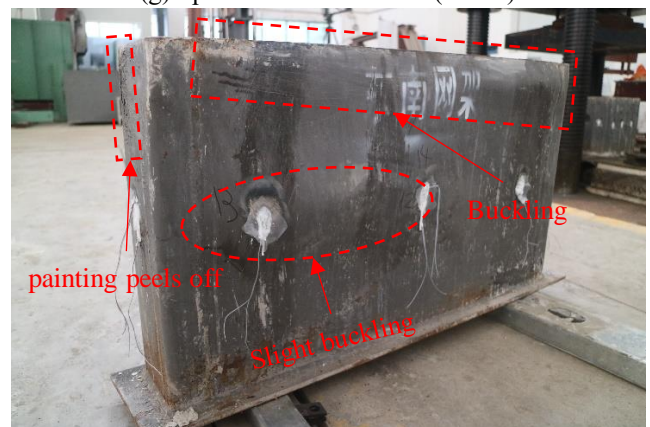
(c) Specimen CWT4W1200 (side S)



(g) Specimen CWT8W900 (side S)



(d) Specimen CWT4W1200 (side N)



(h) Specimen CWT8W900 (side N)

Continued-

Fig. 6 Failure modes

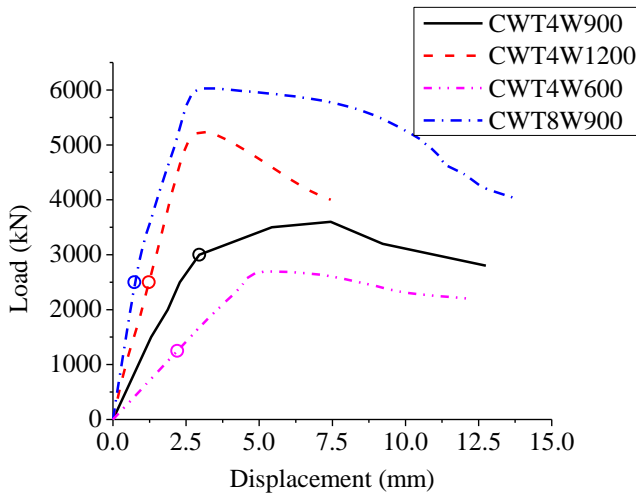


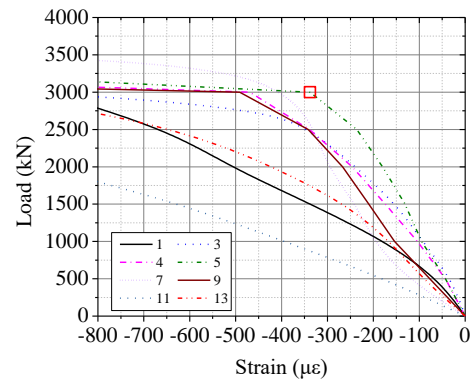
Fig. 7 Load-axial displacement curves

3.2 Load versus axial displacement behavior

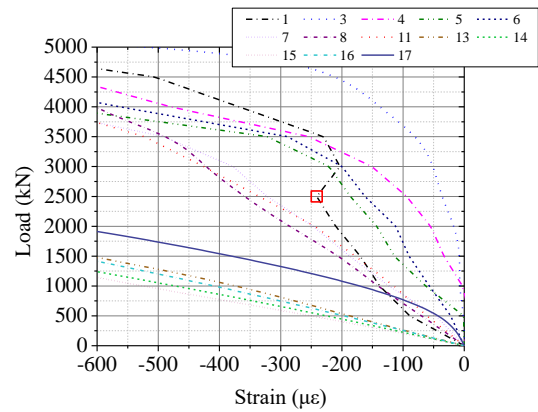
The axial load versus axial displacement behavior of sandwich composite walls under pure compression was shown in Fig. 7. It shows that the specimens experienced three working stages during the test. The first working stage is the elastic stage. During this stage, both steel and concrete are in the elastic range of the material properties. The load-axial displacement curves gradually go up with the increase in axial loading. No obvious deformation could be observed in this stage. The second stage is the elastoplastic stage. During this stage, steel faceplates started to buckle and the concrete started to crush. The specimens exhibited nonlinear behavior. The slope of load-axial displacement curves began to decrease due to the development of plastic deformation. However, the nonlinear behavior of curves varied with different wall width and faceplate thickness. The sandwich composite wall with smaller wall width experienced larger nonlinear behavior than that with larger wall width. In addition, more nonlinear behavior was observed in specimen with smaller faceplate thickness. At the end of this stage, the composite sandwich composite walls reached their ultimate resistance. The third stage is the recession stage. The specimens could not sustain their loading capacities due to the crushing of concrete infill and local buckling of steel faceplates. The stiffness of the specimens changed from positive to negative and the load-axial displacement curves started to climb down. The concrete crushing and local buckling of steel faceplates continued to develop as the axial displacement increased.

3.3 Buckling stress

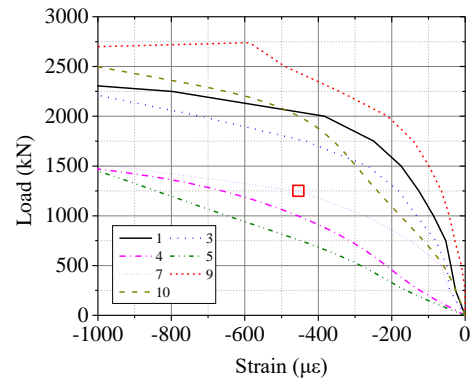
Steel faceplates in sandwich composite walls may experience local buckling due to the thin thickness. In order to investigate the buckling behavior of steel faceplates, several strain gauges have been arranged on the surface of steel plates. The strain values at locations where buckling occurs are expected to change abruptly. In this way the buckling strain can be estimated. It should be noted that due



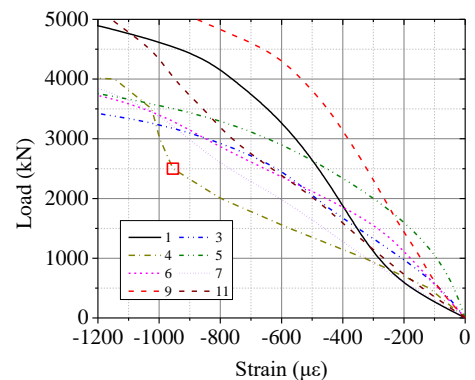
(a) Specimen CWT4W900



(b) Specimen CWT4W1200



(c) Specimen CWT4W600



(d) Specimen CWT8W900

Fig. 8 Determination of buckling strain

to the limitation of numbers of strain gauges used, the estimated buckling strain can only be used to qualitatively evaluate the buckling behavior. However, it is still valuable to assess the restraint condition of steel faceplates in composite walls through this method.

The buckling strain can be approximately determined by the inflection point of the load-strain curves, and the corresponding buckling stress can then be calculated by multiplying the buckling strain by the elastic modulus of steel. Fig. 8 shows the partially-enlarged drawings of load-strain responses for several strains. The buckling points were marked by red squares in the figures. As can be seen from Fig. 8(a), Specimen CWT4W900 has a buckling strain of $338 \mu\epsilon$, and the corresponding buckling stress and buckling load are 67.3 MPa and 3000 kN. Fig. 8(b) shows that Specimen CWT4W1200 has a buckling strain of $241 \mu\epsilon$, and the corresponding buckling stress and buckling load are 48.0 MPa and 2500 kN. It can be found in Fig. 8(c) that Specimen CWT4W600 has a buckling strain of $454 \mu\epsilon$, and the corresponding buckling stress and buckling load are 90.3 MPa and 1250 kN. Fig. 8(d) indicates that Specimen CWT8W900 has a buckling strain of $955 \mu\epsilon$, and the corresponding buckling stress and buckling load are 202.5 MPa and 2500 kN. The buckling load N_b and the corresponding axial displacement d_b were given in Table 2. The buckling load point is also marked in Fig. 7 by circles. It can be seen that except for Specimen CWT4W900, the stiffness of the other specimens does not change significantly after the specimens reach their buckling load.

In order to quantify the restraint condition of steel faceplates, the Euler equation were introduced, as expressed by Eq. (2) (Qin *et al.* 2017). In this equation, the elastic local buckling coefficient k is the parameter to assess the boundary condition of steel faceplates. The value of $k = 1.0$ represents the simply-supported boundary condition, while the value of $k = 0.7$ denotes the clamped boundary condition.

$$\sigma_{cr,Euler} = \frac{\pi^2 E_s}{12k^2 (\bar{B}/t)^2} \quad (2)$$

Fig. 9 shows the relationships between the normalized buckling strain and the normalized slenderness ratio for the tested data. The red dashed line and blue solid line represent the Euler curves with $k = 0.7$ and $k = 1.0$, respectively. Some data from previous tests on sandwich composite wall with shear studs (Akiyama and Sekimoto 1991, Usami *et al.* 1995, Kanchi 1996, Choi and Han 2009) were also included.

It can be seen from Fig. 9 that, the data of Specimen CWT4W900 lies between the two Euler curves, which means that the steel faceplates can be considered as elastically restrained, while the data of Specimen CWT8W900 lies even below the Euler line with $k = 1.0$, which means the restraint of steel faceplates is weaker than simple-supported. This indicated that for sandwich composite wall with thicker steel faceplates, the restraint by steel faceplates is weaker. This can also be verified by the failure modes shown in Fig. 6, where the local buckling occurred between the two adjacent steel trusses in Specimen CWT4W900 while developed across the entire width of wall in Specimen CWT8W900.

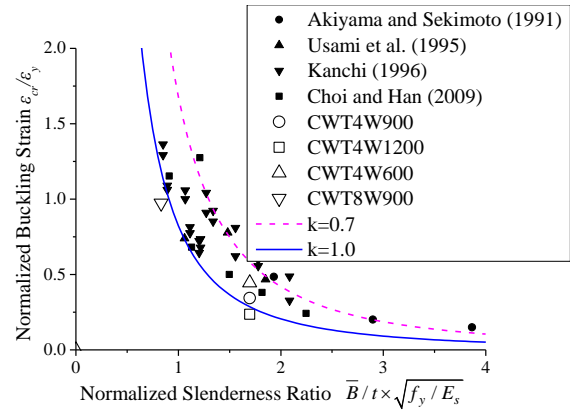


Fig. 9 Comparison with Euler theory

The comparison among Specimens CWT4W900, CWT4W1200, and CWT4W600 shows that the truss connectors could provide better restraint for wall with smaller width. This may be attributed to the relatively stronger restraint by side wall in specimen with smaller width.

3.4 Resistance and stiffness

The ultimate resistance N_u and the corresponding axial displacement d_u were given in Table 2. Compared with Specimen CWT4W600, the ultimate resistance of Specimens CWT4W900 and CWT4W1200 are 31.4% and 100.4%, respectively, higher. The increase in ultimate resistance is mostly contributed from the additional cross-sectional area of wall. Meanwhile, the ultimate strength of Specimen CWT8W900 is 68.1% greater than that of Specimen CWT4W900. This indicated that the increase in thickness of steel faceplates is effective in improving the load-carrying capacity. The increase in ultimate resistance comes from not only the additional steel area but also the enhanced ability to resist local buckling.

In order to further investigate the compressive behavior of the tested walls, the normalized compressive strength of the walls was introduced, which can be calculated as the ratio of the tested ultimate strengths of the walls to the theoretical ultimate strengths. The theoretical strength can be simply taken as the summation of the contribution from steel part and concrete part. The normalized compressive strength of Specimens CWT4W900, CWT4W1200, CWT4W600 and CWT8W900 are 0.73, 0.85, 0.81, and 0.79, respectively. It can be found that the normalized compressive strength firstly decreases as the wall width increases from 600 mm to 900 mm, and then increases as the wall width further grows up to 1200 mm. Meanwhile, the comparison between Specimens CWT4W900 and CWT8W900 shows that the normalized compressive strength goes up with the increase in thickness of steel faceplate.

The points corresponding to $0.1N_u$, $0.2N_u$ and $0.3N_u$ are used to calculate the initial stiffness. The average initial stiffness K_i for Specimens CWT4W900, CWT4W1200, CWT4W600 and CWT8W900 are 1151 kN/mm, 2225 kN/mm, 568 kN/mm, and 3409 kN/mm, respectively. It can also be found

Table 2 Test results

Specimen	N_b	d_b	N_u	d_u	K_i	μ	SI
	kN	mm	kN	mm	kN/mm		
CWT4W900	3000	2.95	3600	7.44	1151	1.40	0.73
CWT4W1200	2500	1.23	5490	3.02	2225	1.73	0.85
CWT4W600	1250	2.20	2740	4.71	568	2.06	0.81
CWT8W900	2500	0.73	6050	3.21	3409	3.24	0.79

that increasing the thickness of steel faceplates rather than the wall width is more efficient in improving the initial stiffness.

3.5 Ductility ratio and strength index

Ductility ratio (μ) is defined as the ratio of the axial displacement corresponding to $0.85N_u$ during the recession stage to the axial displacement corresponding to N_u (Xiong *et al.* 2017). The calculated ductility ratio for each specimen was listed in Table 2. It can be seen that Specimen CWT8W900 with thicker faceplates has the highest ductility ratio, which means the wall is able to undergo the greatest plastic deformation without significant loss of loading capacity.

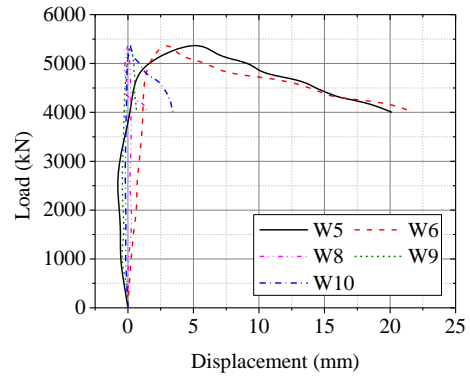
Strength index (SI) is used to evaluate the utilization of cross-sectional resistance of the sandwich composite walls (Huang and Liew 2016). It can be calculated by the ratio of the ultimate resistance N_u of the wall to the fully-utilized resistance N_f . The expression is shown in Eq. (3). The calculated strength index was shown in Table 2. It can be noticed that the Specimen CWT4W1200 has the highest strength index. This indicated that the walls with larger width could better develop its yield strength under axial compression.

$$SI = \frac{N_u}{N_f} = \frac{N_u}{f_y A_s + f_c A_c} \quad (3)$$

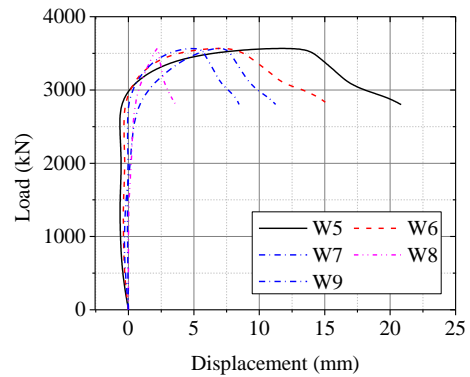
3.6 Load-lateral deformation responses

The relationships between axial load and lateral deformation were shown in Fig. 10. All specimens exhibited similar load-lateral deformation behavior. The lateral deformation slowly and mostly linearly climbed up as the axial loading increased during the elastic stage. The lateral deformation started to grow faster when the local buckling developed in the wall, as was evidenced by the change in slope of the curves. During the recession stage, the lateral deformation quickly increased at a higher rate.

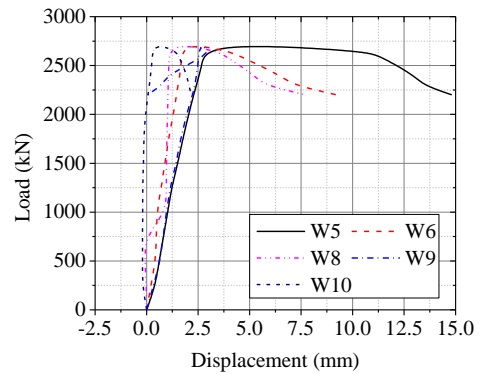
The comparison among specimens showed that Specimen CWT8W900 had the smallest lateral deformation. This is because the thick steel faceplates prevent premature local buckling and thus reduce the out-of-plane deflection. Specimen CWT4W1200 had larger lateral deformation than Specimens CWT4W900 and CWT4W600. This can be explained by the fact that Specimen CWT4W1200 had the greatest wall width, which provided the weakest restraint to external faceplates.



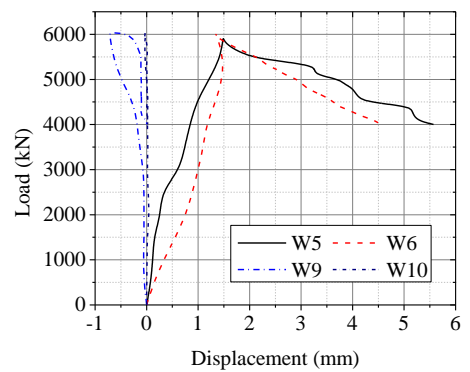
(a) Specimen CWT4W900



(b) Specimen CWT4W1200

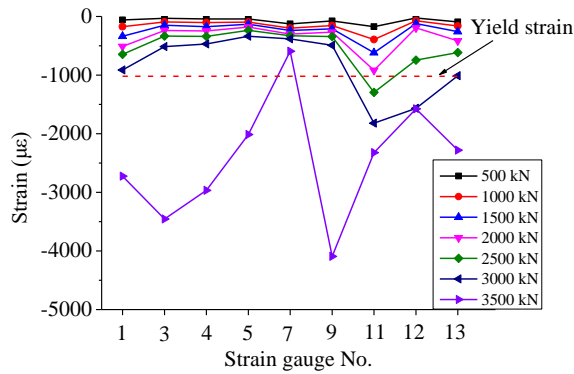


(c) Specimen CWT4W600

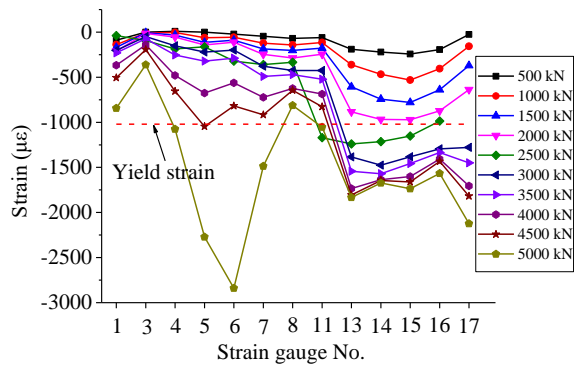


(d) Specimen CWT8W900

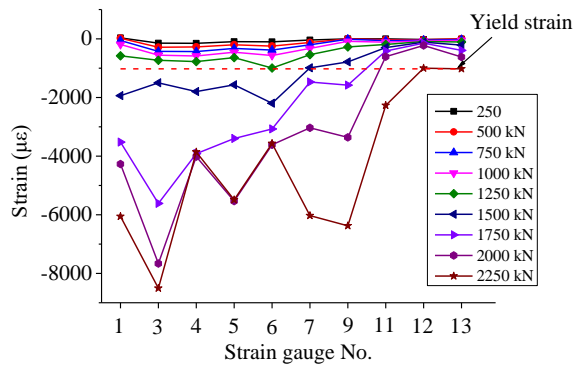
Fig. 10 Load-lateral deformation curves



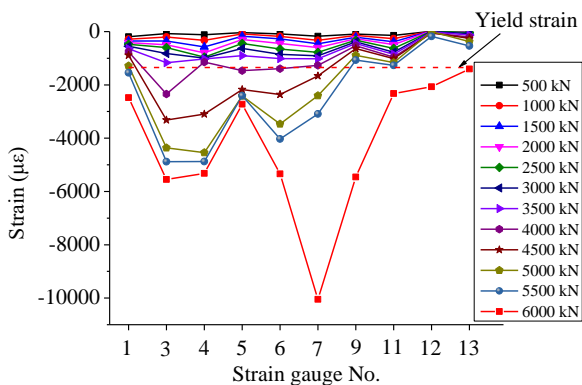
(a) Specimen CWT4W900



(b) Specimen CWT4W1200



(c) Specimen CWT4W600



(d) Specimen CWT8W900

Fig. 11 Strain distribution

3.7 Load-strain responses

Fig. 11 illustrated the strain distribution across the wall section based on each loading level. The yield strain was marked by red dashed line. It can be seen that the strains are mostly distributed uniformly across the entire section during the first several loading steps. The strain distribution started to become un-uniform as the local buckling progressed in the steel faceplates, which caused strain redistribution in the wall.

For specimens with the same thickness of steel faceplates, the wall with smaller width yielded earlier than the wall with larger width. This is because under the same loading level, more part of axial compression had been transferred to the concrete core in sandwich composite wall with greater width. Meanwhile, it can be observed that the strain distribution in Specimen CWT8W900 is more uniform than in other three specimens. This can be attributed to the fact the thicker steel faceplates were able to prevent premature local buckling and thus avoid the strain redistribution.

4. Code-based design

4.1 AISC 360-16

The design equations for predicting the compressive strength of axially loaded doubly symmetric filled composite members are incorporated in AISC 360-16 (2016). It is assumed that the steel plates reach their buckling strength f_{cr} while the concrete reach $0.7f_c$, as can be given by Eq. (4). The buckling strength f_{cr} can be calculated by Eq. (5) for rectangular filled sections.

$$N_{AISC} = f_{cr}A_s + 0.7f_cA_c \quad (4)$$

$$f_{cr} = \frac{9E_s}{(b/t)^2} \quad (5)$$

4.2 EN 1994-1-1

Eurocode 4 (EN 1994-1-1, 2004) assumes that the steel faceplates develop their yield strength of f_y . Meanwhile, the concrete is able to reach $0.85f_c$, which can be expressed by Eq. (6).

$$N_{EC4} = f_yA_s + 0.85f_cA_c \quad (6)$$

4.3 CECS 159

CECS 159 (2004) considers that the steel reaches its yield strength of f_y . Meanwhile, concrete core is assumed to be well confined and reach its compressive strength of f_c , which can be calculated by Eq. (7).

$$N_{CECS} = f_yA_s + f_cA_c \quad (7)$$

4.4 Discussion

The calculated results by these modern codes were given in Table 3. It should be noted that the cylinder compressive

Table 3 Predictions by modern codes

Specimen No.	N_{AISC}	N_{EC4}	N_{CECS}	$\frac{N_u}{N_{AISC}}$	$\frac{N_u}{N_{EC4}}$	$\frac{N_u}{N_{CECS}}$
	kN	kN	kN			
CWT4W900	1721	4607	4911	2.09	0.78	0.73
CWT4W1200	2115	6017	6423	2.60	0.91	0.85
CWT4W600	1426	3197	3399	1.92	0.86	0.81
CWT8W900	3727	7335	7620	1.62	0.82	0.79
Average				2.06	0.84	0.80
Standard deviation				0.353	0.048	0.043

strength of concrete was used to calculate the theoretical ultimate strength of the walls. The differences among the three codes mainly lie in two factors. The first is the strength of steel which is used. The second is the partial factor of the concrete part. It can be seen that the average and standard deviation of the ratio between test results and predictions by AISC are 2.06 and 0.353, respectively. The reason AISC significantly underestimates the ultimate resistance is that AISC largely underestimates the strength of steel faceplates. It can also be found that Eurocode 4 provides the most suitable results with the average N_u/N_{CECS} ratio of 0.84 and standard deviation of 0.048. It can also be observed that Eurocode 4 and CECS 159 overestimate the compressive strength of the walls. The reason may be caused by the fact that the steel may not be able to reach its yield strength. In addition, the premature buckling of steel faceplate weakens the confinement to concrete, which may result in the reduction in concrete strength.

5. Conclusions

In this paper, a new type of sandwich composite wall system proposed by Qin *et al.* (2019a) was studied. Steel truss was proposed as the internal mechanical connector to bond the steel faceplate to concrete core. Compressive tests were performed on four specimens with varied wall width and faceplate thickness. The following conclusions can be drawn based on the test results.

- All specimens were failed by cross-sectional capacity. No global buckling was observed during the test. The specimens showed high resistance, good ductility, and reasonable strength index.
- Truss connectors could provide better restraints to steel faceplates in sandwich composite wall with thinner faceplate thickness or smaller wall width. In contrast, Stress distribution is more uniform in sandwich composite wall with thicker faceplate thickness or larger wall width.
- Increasing the faceplate thickness rather than the wall width is more effective in improving the ultimate resistance and axial stiffness of the wall.
- AISC greatly underestimates the actual resistance of the proposed wall, while Eurocode 4 and CECS offers overestimations.

Acknowledgments

This work is sponsored by the Natural Science Foundation of Jiangsu Province (Grant No. BK20170685), and the National Key Research and Development Program of China (Grant No. 2017YFC0703802). The authors would like to thank the Zhejiang Southeast Space Frame Group Company Limited for the supply of test specimens, and Xiongliang Zhou, Weigang Chen, Yunfei He and Jianwei Ni for their assistance with the specimen fabrication.

References

- AISC 360-16 (2016), Specification for structural steel buildings, American Institute of Steel Construction, Chicago, USA.
- Akiyama, H. and Sekimoto, H. (1991), "A compression and shear loading tests of concrete filled steel bearing wall", *Transaction of 11th Structural Mechanics in Reactor Technology (SMiRT-11)*, Tokyo, Japan, August.
- Ayazi, A. and Shafaei, S. (2019), "Steel-concrete composite shear walls using precast high performance fiber reinforced concrete panels", *Struct. Des. Tall Spec. Build.*, **28**(10), e1617. <https://doi.org/10.1002/tal.1617>.
- Bafti, F.G., Mortezaei, A. and Kheyroddin, A. (2019), "The length of plastic hinge area in the flanged reinforced concrete shear walls subjected to earthquake ground motions", *Struct. Eng. Mech.*, **69** (6), 651-665. <https://dx.doi.org/10.12989/sem.2019.69.6.651>.
- Beiraghi, H. (2019), "Seismic response of dual structures comprised by Buckling-Restrained Braces (BRB) and RC walls", *Struct. Eng. Mech.*, **72** (4), 443-454. <https://dx.doi.org/10.12989/sem.2019.72.4.443>.
- Bruhl, J.C. and Varma, A.H. (2018), "experimental evaluation of steel-plate composite walls subject to blast loads", *J. Struct. Eng.*, **144**(9), 04018155. [https://doi.org/10.1061/\(ASCE\)ST.1943-541X.0002163](https://doi.org/10.1061/(ASCE)ST.1943-541X.0002163).
- CECS 159 (2004), Technical specification for structures with concrete-filled rectangular steel tube members; China Association for Engineering Construction Standardization, Beijing, China.
- Chen, L., Mahmoud, H., Tong, S.M. and Zhou, Y. (2015), "Seismic behavior of double steel plate-HSC composite walls", *Eng. Struct.*, **102**, 1-12. <http://dx.doi.org/10.1016/j.engstruct.2015.08.017>.
- Chen, L., Wang, S., Lou, Y. and Xia, D. (2019), "Seismic behavior of double-skin composite wall with L-shaped and C-shaped connectors", *J. Constr. Steel Res.*, **160**, 255-270. <https://doi.org/10.1016/j.jcsr.2019.05.033>.
- Choi, B.J. and Han, H.S. (2009), "An experiment on compressive profile of the unstiffened steel plate-concrete structures under compression loading", *Steel Compos. Struct.*, **9**(6), 519-534. <https://doi.org/10.12989/scs.2009.9.6.519>.
- Choi, B.J., Kang, C.K. and Park, H.Y. (2014), "Strength and behavior of steel plate-concrete wall structures using ordinary and eco-oriented cement concrete under axial compression", *Thin Wall Struct.*, **84**, 313-324. <http://dx.doi.org/10.1016/j.tws.2014.07.008>.
- Curkovic, I., Skejic, D., Dzeba, I and De Matteis, G. (2019), "Seismic performance of composite plate shear walls with variable column flexural stiffness", *Steel Compos. Struct.*, **33**(1), 851-868. <https://doi.org/10.12989/scs.2019.33.1.851>.
- Deifalla, A.F., Fattouh, F.M., Fawzy, M.M. and Hussein, I.S. (2019), "Behavior of stiffened and unstiffened CFT under concentric loading, An experimental study", *Steel Compos. Struct.*, **33**(6), 793-803. <https://doi.org/10.12989/scs.2019.33.793>.

- EN 1994-1-1 (2004), Eurocode 4: Design of composite steel and concrete structures-Part 1-1: General rules and rules for buildings, European Standard Institute, Brussels, Belgium.
- Eom, T.S., Park, H.G., Lee, C.H., Kim, J.H. and Chang, I.H. (2009), "Behavior of double skin composite wall subjected to in-plane cyclic loading", *J. Struct. Eng.*, **135**(10), 1239-1249. [http://dx.doi.org/10.1061/\(ASCE\)ST.1943-541X.0000057](http://dx.doi.org/10.1061/(ASCE)ST.1943-541X.0000057).
- GB50010-2010 (2015), Code for design of concrete structures; China Architecture & Building Press, Beijing, China.
- Guo, Q. and Zhao, W. (2019), "Design of steel-concrete composite walls subjected to low-velocity impact", *J. Constr. Steel Res.*, **154**, 190-196. <https://doi.org/10.1016/j.jcsr.2018.12.001>.
- Guo, L., Wang, Y. and Zhang, S. (2018), "Experimental study of rectangular multi-partition steel-concrete composite shear walls", *Thin Wall Struct.*, **130**, 577-592. <https://doi.org/10.1016/j.tws.2018.06.011>.
- Hossain, K.M.A. and Wright, H.D. (2004), "Behaviour of composite walls under monotonic and cyclic shear loading", *Struct. Eng. Mech.*, **17**(1), 69-85. <http://dx.doi.org/10.12989/sem.2004.17.1.069>.
- Hu, H.S., Nie, J.G. and Eatherton, M.R. (2014), "Deformation capacity of concrete-filled steel plate composite shear walls", *J. Constr. Steel Res.*, **103**, 148-158. <http://dx.doi.org/10.1016/j.jcsr.2014.08.006>.
- Huang, S.T., Huang, Y.S., He, A., Tang, X.L., Chen, Q.J., Liu, X. and Cai, J. (2018), "Experimental study on seismic behaviour of an innovative composite shear wall", *J. Constr. Steel Res.*, **148**, 165-179. <https://doi.org/10.1016/j.jcsr.2018.05.003>.
- Huang, Z.Y. and Liew, J.Y.R. (2016), "Structural behaviour of steel-concrete-steel sandwich composite wall subjected to compression and end moment", *Thin Wall Struct.*, **98**, 592-606. <http://dx.doi.org/10.1016/j.tws.2015.10.013>.
- Ji, X., Cheng, X., Jia, X. and Varma, A.H. (2017), "cyclic in-plane shear behavior of double-skin composite walls in high-rise buildings", *J. Struct. Eng.*, **143**(6), 04017025. [http://dx.doi.org/10.1061/\(ASCE\)ST.1943-541X.0001749](http://dx.doi.org/10.1061/(ASCE)ST.1943-541X.0001749).
- Liu, Z.A., Liu, H.B., Chen, Z.H. and Zhang, G.P. (2018), "Structural behavior of cold-formed thick-walled rectangular steel columns", *J. Constr. Steel Res.*, **147**, 277-292. <http://dx.doi.org/10.1016/j.jcsr.2018.03.013>.
- Kanchi, M. (1996), "Experimental study on a concrete filled steel structure Part 2 Compressive tests (1). Summary of Technical Papers of Annual Meeting", Architectural Institute of Japan, 1996, 1071-1072.
- Mydin, M.A.O. and Wang, Y.C. (2011), "Structural performance of lightweight steel-foamed concrete-steel composite walling system under compression", *Thin Wall Struct.*, **49**, 66-76. <http://dx.doi.org/10.1016/j.tws.2010.08.007>.
- Nguyen, N.H. and Whittaker, A.S. (2017), "Numerical modelling of steel-plate concrete composite shear walls", *Eng. Struct.*, **150**, 1-11. <http://dx.doi.org/10.1016/j.engstruct.2017.06.030>.
- Nie, J.G., Ma, X.W., Tao, M.X., Fan, J.S. and Bu, F.M. (2014), "Effective stiffness of composite shear wall with double plates and filled concrete", *J. Constr. Steel Res.*, **99**, 140-148. <http://dx.doi.org/10.1016/j.jcsr.2014.04.001>.
- Prabha, P., Marimuthu, V., Saravanan, M., Palani, G.S., Lakshmanan, N. and Senthil, R. (2013), "Effect of confinement on steel-concrete composite light-weight load-bearing wall panels under compression", *J. Constr. Steel Res.*, **81**, 11-19. <http://dx.doi.org/10.1016/j.jcsr.2012.10.008>.
- Qin, Y., Shu, G.P., Fan, S.G., Lu, J.Y., Cao, S. and Han, J.H. (2017), "Strength of double skin steel-concrete composite walls", *Int. J. Steel Struct.*, **17**(2), 535-541. <http://dx.doi.org/10.1007/s13296-017-6013-9>.
- Qin, Y., Shu, G.P., Zhou, G.G. and Han, J.H. (2019a), "Compressive behavior of double skin composite wall with different plate thicknesses", *J. Constr. Steel Res.*, **157**, 297-313. <https://doi.org/10.1016/j.jcsr.2019.02.023>.
- Qin, Y., Shu, G.P., Zhou, G.G., Han, J.H. and Zhou, X.L. (2019b), "Truss spacing on innovative composite walls under compression", *J. Constr. Steel Res.*, **160**, 1-15. <https://doi.org/10.1016/j.jcsr.2019.05.027>.
- Qin, Y., Chen, X., Xi, W., Zhu, X.Y. and Chen, Y.Z. (2020), "Compressive behavior of rectangular sandwich composite wall with different truss spacings", *Steel Compos. Struct.*, **34**(6), 783-794. <https://doi.org/10.12989/scs.2020.34.6.783>.
- Rafiei, S., Hossain, K.M.A., Lachemi, M. and Behdinan, K. (2017), "Impact shear resistance of double skin profiled composite wall", *Eng. Struct.*, **140**, 267-285. <http://dx.doi.org/10.1016/j.engstruct.2017.02.062>.
- Song, Y., Uy, B. and Wang, J. (2019), "Numerical analysis of stainless steel-concrete composite beam-to-column joints with bolted flush endplates", *Steel Compos. Struct.*, **33**(1), 975-994. <http://dx.doi.org/10.12989/scs.2019.33.1.975>.
- Seo, J., Varma, A.H., Sener, K. and Ayhan, D. (2016), "Steel-plate composite (SC) walls: In-plane shear behavior, database, and design", *J. Constr. Steel Res.*, **119**, 202-215. <http://dx.doi.org/10.1016/j.jcsr.2015.12.013>.
- Usami, S., Akiyama, H., Narikawa, M., Hara, K., Takeuchi, M. and Sasaki, N. (1995), "Study on a concrete filled steel structure for nuclear plants (part 2). Compressive loading tests on wall members", *Transaction of 13th Structural Mechanics in Reactor Technology (SMIRT-13)*, Porto Alegre, Brazil, August.
- Varshney, L.K., Patel, K.A., Chaudhary, S. and Nagpal, A.K. (2019), "An efficient and novel strategy for control of cracking, creep and shrinkage effects in steel-concrete composite beams", *Struct. Eng. Mech.*, **70** (6), 751-763. <https://dx.doi.org/10.12989/sem.2019.70.6.751>.
- Wei, F., Zheng, Z., Yu, J. and Wang, Y. (2019), "Structure behavior of concrete filled double-steel-plate composite walls under fire", *Adv. Struct. Eng.*, **22**(8), 1895-1908. <https://doi.org/10.1177/1369433218825238>.
- Xiong, Q.Q., Chen, Z.H., Zhang, W., Du, Y.S., Zhou, T. and Kang, J.F. (2017), "Compressive behaviour and design of L-shaped columns fabricated using concrete-filled steel tubes", *Eng. Struct.*, **152**, 758-770. <https://doi.org/10.1016/j.engstruct.2017.09.046>.
- Yan, J.B., Wang, Z., Wang, T. and Wang, X.T. (2018), "Shear and tensile behaviors of headed stud connectors in double skin composite shear wall", *Steel Compos. Struct.*, **26**(6), 759-769. <https://doi.org/10.12989/scs.2018.26.6.759>.
- Yan, J.B., Chen, A.Z. and Wang, T. (2019), "Developments of double skin composite walls using novel enhanced C-channel connectors", *Steel Compos. Struct.*, **33**(6), 877-889. <https://doi.org/10.12989/scs.2019.33.6.877>.
- Yang, Y., Xue, Y.C., Zhang, T. and Tian, J. (2018), "Structural performance of GFRP-concrete composite beams", *Struct. Eng. Mech.*, **68** (4), 485-495. <https://dx.doi.org/10.12989/sem.2018.68.4.485>.
- Zhou, T., Ren, Z., Jiang, B., Xu, M., Lei, Z. and Chen, Z. (2019), "Calculating Method Study and Parameter Analysis of Slender LCFST Columns Under Axial Loading", *Int. J. Steel Struct.*, **19**(5), 1645-1661. <http://dx.doi.org/10.1007/s13296-019-00234-2>.
- Zhao, W., Guo, Q., Huang, Z., Tan, L., Chen, J. and Ye, Y. (2016), "Hysteretic model for steel-concrete composite shear walls subjected to in-plane cyclic loading", *Eng. Struct.*, **106**, 461-470. <http://dx.doi.org/10.1016/j.engstruct.2015.10.031>.